

# BiDepth Multimodal Neural Network: Bidirectional Depth Deep Learning Architecture for Spatial-Temporal Prediction

Sina Ehsani<sup>1,2\*</sup>, Fenglian Pan<sup>1</sup>, Qingpei Hu<sup>3</sup>, Jian Liu<sup>1\*</sup>

<sup>1</sup> Department of Systems and Industrial Engineering, University of Arizona, Tucson, 85721, Arizona, USA.

<sup>2</sup> AI Research, Armada, San Francisco, 94129, CA, USA.

<sup>3</sup> Academy of Mathematics and Systems Science, Chinese Academy of Sciences, Beijing, 100190, Beijing, China.

\*Corresponding author(s). E-mail(s): [sinaehsani@arizona.edu](mailto:sinaehsani@arizona.edu);  
[jianliu@arizona.edu](mailto:jianliu@arizona.edu);

Contributing authors: [fenglianpan@arizona.edu](mailto:fenglianpan@arizona.edu); [qingpeihu@amss.ac.cn](mailto:qingpeihu@amss.ac.cn);

## Abstract

Accurate prediction of spatial-temporal (ST) information in dynamic systems, such as urban mobility and weather patterns, is a crucial yet challenging problem. The complexity stems from the intricate interplay between spatial proximity and temporal relevance, where both long-term trends and short-term fluctuations are present in convoluted patterns. Existing approaches, including traditional statistical methods and conventional neural networks, may provide inaccurate results due to the lack of an effective mechanism that simultaneously incorporates information at variable temporal depths while maintaining spatial context, resulting in a trade-off between comprehensive long-term historical analysis and responsiveness to short-term new information. To bridge this gap, this paper proposes the BiDepth Multimodal Neural Network (BDMNN) with bidirectional depth modulation that enables a comprehensive understanding of both long-term seasonality and short-term fluctuations, adapting to the complex ST context. Case studies with real-world public data demonstrate significant improvements in prediction accuracy, with a 12% reduction in Mean Squared Error for urban traffic prediction and a 15% improvement in rain precipitation forecasting compared to state-of-the-art benchmarks, without demanding extra computational resources.

**Keywords:** Multimodal Neural Network, Spatial-Temporal, Traffic Prediction, Weather Forecasting

# 1 Introduction

Spatio-temporal (ST) data, characterized by observations that vary spanning both spatial and temporal continuum, have become increasingly prevalent and critical in various domains, such as climate science (Aburas et al, 2019), urban planning (Song et al, 2019; Xia et al, 2025), transportation (Ling et al, 2023; Ehsani et al, 2024), and environmental monitoring (Amato et al, 2020). These datasets capture complex (ST) dynamics, offering valuable insights into evolving patterns and trends. A prime example is the New York City (NYC) Taxi and Limousine Commission Trip Record Data (“TLC data” hereafter - refer to Section 3.1.1 for details on this dataset.), which provides detailed information on taxi trips, including pick-up and drop-off locations, times, and associated attributes (NYC Taxi and Limousine Commission, 2024). The analysis of such ST data is crucial for understanding urban mobility patterns, optimizing transportation systems, and informing policy decisions (Zhou and Hirasawa, 2019).

The inherent complexity of ST data presents significant challenges for analysis and forecasting (Yuan and Li, 2021), stemming from their unique ST characteristics manifested as spatial and temporal correlations. **Spatial correlations** imply that observations at certain locations tend to be more inter-related than those at other locations, creating complex spatial patterns (Li et al, 2017). For example, in the TLC Data, taxi demands in one neighborhood often correlates with demands in adjacent neighborhoods. **Temporal correlations** refer to the inter-relationship between successive data points, with the influence from historical values varying based on temporal proximity. For instance, a surge in taxi pickups at a particular time is likely to be influenced by the pickups in preceding time intervals. The spatial and temporal interaction (**ST correlations**) creates intricate patterns, making it critical yet difficult to build models that can simultaneously capture both aspects without losing critical information. For example, in the TLC data, higher taxi pickups in outlying areas in the early morning can indicate increased demand in Midtown during evening rush hour.

Additionally, ST data exhibits non-stationary and multi-scale dynamics, characterized by short-term fluctuations and long-term trends that vary over multiple spatial and temporal scales simultaneously (Lai et al, 2018). **Short-term fluctuations** refer to immediate, transient changes in the data, such as daily peaks in taxi demand during morning and evening rush hours. **Long-term trends** denote the overall direction or movement in the data over extended periods, such as seasonal variations or a gradual increase in taxi usage over several years due to population growth. These evolving non-stationary patterns add another layer of complexity to modeling ST data, as models must adapt to changes over both short and long-term periods. Furthermore, ST data often exhibit **high dimensionality** due to the combination of numerous spatial locations and time intervals, increasing computational complexity (Geng et al, 2019). For example, the NYC TLC data divides the city into over 200 taxi zones, and data is collected over several years, resulting in high-dimensional data matrices where each dimension represents a spatial location at a specific time.

Facing the challenges posed by these ST characteristics — ST correlation complexity, non-stationary patterns, and high dimensionality — the goal of this research is to

develop a predictive model that can effectively capture these challenging ST characteristics. Specifically, our goal is to design a multimodal neural network architecture that balances the analysis of both short-term fluctuations and long-term trends in ST prediction. This architecture should be able to process high-dimensional data efficiently while incorporating spatial information effectively without compromising the temporal or spatial context in our prediction model.

Numerous methods have been proposed in recent decades for spatiotemporal (ST) data predictions, which can generally be categorized into traditional statistical methods (Cressie and Wikle, 2011) and machine learning (ML) (Shi and Yeung, 2018) or deep learning (DL) (Wang et al, 2020) approaches. Traditional statistical models, such as the Auto-Regressive Integrated Moving Average (ARIMA) and its variants (Shekhar and Williams, 2007; Li et al, 2012; Adhikari and Agrawal, 2013; Moreira-Matias et al, 2013), have been widely applied for ST prediction tasks. Recent studies have incorporated spatial relations and external contextual data (Tong et al, 2017; Deng et al, 2016) to enhance time series predictions. Although these studies demonstrate that predictions can be improved by considering additional factors, they often fail to capture complex ST correlations effectively (Yao et al, 2018). To address the challenges of modeling ST correlations, multivariate Poisson log-normal models have been proposed (Xian et al, 2021; Yang et al, 2024). However, these methods are constrained by their reliance on predefined covariance structures and struggle with scalability in high-dimensional, non-stationary contexts.

Recent advances in ML and DL have enabled researchers to model complex ST correlations, yielding promising results across various fields (LeCun et al, 2015). This progress has inspired several attempts to apply ML/DL techniques to ST prediction problems. Among the most commonly used ML methods are k-nearest neighbors (kNN) and support vector machines (SVMs). For example, (Arroyo and Maté, 2009) adapted the kNN algorithm to forecast histogram data, particularly histogram time series, by utilizing the Mallows distance and the Wasserstein distance. (Marchang and Tripathi, 2020) integrated ST correlations into the kNN method for missing data inference in environmental crowd sensing. Additionally, (Feng et al, 2018) employed a multi-kernel SVM approach with ST correlations for short-term traffic flow prediction. While these methods capture ST correlations to some extent, they remain highly sensitive to the selection of the distance metric (kNN) and kernel function (SVM). Furthermore, they generally struggle to model non-stationary patterns in ST data and face significant computational challenges as data dimensionality increases. To mitigate scalability issues, DL methods have been proposed as a robust alternative.

Convolutional Neural Networks (CNNs) (Ali et al, 2022; Casallas et al, 2022), such as U-Net (Ronneberger et al, 2015), excel at capturing spatial patterns but lack inherent temporal sensitivity (He et al, 2019). Recurrent Neural Networks (RNNs) and Long Short-Term Memory networks (LSTMs) (Hochreiter and Schmidhuber, 1997) effectively model temporal correlations (Zenkner and Navarro-Martinez, 2023) but face challenges in processing spatial data (Shi et al, 2015). To capture the ST correlation complexity simultaneously, multimodal neural networks have been proposed. Hybrid CNN-RNN architectures, such as those by Lu et al (2020), attempt to capture both spatial and temporal dependencies by integrating convolutional layers with

recurrent units. However, they may still struggle with capturing complex long-range temporal dependencies and intricate spatio-temporal interactions inherent in ST data. Shi et al (2015) proposed the ConvLSTM to integrate convolutional operations into LSTMs, addressing some spatial aspects. However, ConvLSTM still faces challenges with efficiently modeling non-stationary patterns when balancing short-term fluctuations with long-term trends. Models like LSTNet (Lai et al, 2018) and the Vision Transformer (ViViT) (Arnab et al, 2021) attempt to capture spatio-temporal patterns using CNN-LSTM hybrids and self-attention mechanisms, respectively. However, both approaches rely heavily on flattening the spatial dimensions, which results in the loss of critical spatial correlations. This limitation undermines their ability to fully preserve and model the intricate spatial dependencies inherent in ST data. Other approaches (Salekin et al, 2021; Zhang et al, 2022) aim to combine different types of data or models to capture both spatial and temporal aspects, but they may not fully address the complexity of non-stationary patterns in high-dimensional ST data.

**Table 1** Comparison of ST prediction approaches

ST characteristic	Traditional Statistical Method		Traditional ML/DL-based Method		Proposed Method
	ARIMA-based	Poisson Process-based	ML-based	DL-based	
High dimensionality	No	No	No	<b>Yes</b>	<b>Yes</b>
Complex ST correlations	No	<b>Yes</b>	<b>Yes</b>	<b>Yes</b>	<b>Yes</b>
Non-stationary patterns	No	No	No	No	<b>Yes</b>

Table 1 summarizes the limitations of the representative state-of-the-art methods in capturing the ST characteristics: high dimensionality, complex ST correlations, and non-stationary patterns. To address these limitations, we propose the BiDepth Multimodal Neural Network (BDMNN), a deep learning architecture designed for ST prediction. The BDMNN introduces a dual-depth structure through its complementary components, allowing for depth modulation based on temporal, and incorporates mechanisms to model high-dimensional spatial correlations explicitly. Specifically, this paper makes the following methodological contributions:

- **To capture the complex ST correlation**, a convolutional self-attention cell (CSAC) is proposed to preserve spatial correlations throughout the network, enabling more effective modeling of spatial correlations while considering the evolving temporal correlations.
- **To handle the non-stationary patterns**, a BiDepth mechanism that adjusts the depth of the network based on temporal context is proposed, allowing it to balance short-term fluctuations and long-term trends effectively.
- **To enhance efficiency in high-dimensional data**, a weight-sharing mechanism that reduces the number of parameters and prevents overfitting is incorporated into the BDMNN, improving generalization across different time steps.

The remainder of this paper is structured as follows. In Section II, we introduce the BiDepth architecture, encompassing its theoretical underpinnings and implementation specifics. Section III presents case studies, preprocessing techniques, results, and performance comparisons. Section IV concludes the paper by discussing the implications of our findings and outlining future research directions in this rapidly evolving field.

## 2 Methodology

The BDMNN, delineated in this section, presents a novel method to navigate the intricate corridors of ST data analysis, addressing methodological gaps in the existing analytical models. Centralized around two pivotal components—the BiDepth Encoder and the TimeSeries Encoder — graphically illustrated in Figure 1. Initially, we present a brief overview of the entire operation, followed by a detailed exploration of each individual component.

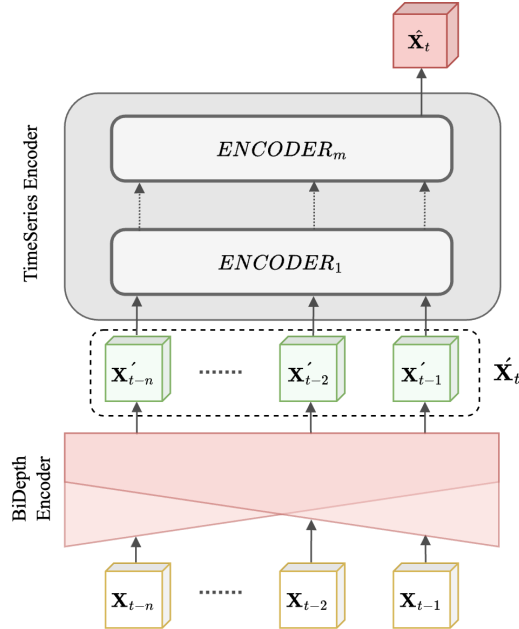


**Fig. 1** Overview of the BDMNN. The data is processed through the BiDepth Encoder, resulting in spatially transformed sequences. These sequences are then passed to the TimeSeries Encoder, which captures the temporal dynamics and produces the prediction for the target timestamp.

At the core of this framework is the BiDepth Encoder, which orchestrates the processing of each timestamp within a given sequence through convolutional layers. The Encoder integrates the BDMNN’s dual aspects: a DeepShallow network and a ShallowDeep network. The DeepShallow network employs a decreasing layer depth along the temporal context, which reduces the layer depth for recent data and thus enables swift adaptation to new information, while the ShallowDeep network does the opposite, applying increased depth to recent data to capture complex, short-term dependencies. The rationale behind this BiDepth approach stems from the characteristics of ST data, where relationships between variables can vary in complexity over time and space. For instance, in the TLC data, taxi demand may have direct and straightforward relationships with recent past data at a local level—the demand in a specific neighborhood in the previous hour may closely predict the current demand. However, there may also be complex recent events, such as sudden traffic congestion due to an

accident, that require a more complex model structure (i.e., deeper layers) to capture non-linear and intricate dependencies across a broader spatial area. Non-linear dependencies refer to relationships that cannot be captured by linear models, often arising from high-dimensionality and non-stationarity in the data. By using both decreasing and increasing layer depths, the model can capture simple, localized direct relations with shallow layers (simpler model structure) and more complex, overall spatial patterns with deeper layers. Similarly, for longer-term dependencies, sometimes simple patterns like weekly seasonality (e.g., higher demand on Friday evenings in certain neighborhoods) can be captured with shallow layers focused on localized trends, while other times, more complex seasonal patterns (e.g., city-wide changes due to holidays or special events) require deeper layers to model effectively across the entire spatial domain. If we were to use only one directional depth assignment, we might miss capturing either the simple, localized relationships or the complex, global dependencies, leading to suboptimal performance. An equal depth approach may not provide the flexibility needed to adapt to varying complexities in the data over different time scales and spatial scales. Our experiments, as discussed in Section 3.3, demonstrate that the BiDepth approach outperforms single-directional (i.e. DeepShallow (Ehsani and Liu, 2024) or ShallowDeep) or equal-depth architectures (i.e. ConvLSTM (Shi et al, 2015) or ViViT (Arnab et al, 2021) ) in capturing the diverse temporal and spatial patterns present in ST data.

This combination of layer depth, alternating between the DeepShallow and ShallowDeep methodologies, allows the model to proficiently handle the intricate demands of ST data analysis. This flexible architecture not only adjusts to the varying complexity of the data but also ensures comprehensive processing of both historical and recent data, offering a nuanced understanding of the entire temporal spectrum.

As illustrated in Figure 1, we represent our ST data as a tensor  $\mathbf{X} \in \mathbb{R}^{b \times n \times c \times h \times w}$ . Here,  $b$  denotes the batch size, indicating the number of samples processed in parallel;  $n$  is the number of historical time steps (i.e., the window size), reflecting how many previous time intervals are considered,  $c$  represents the number of feature channels at each spatial location, such as 15-minute intervals capturing events like rush hours (e.g.,  $c = 16$  for a 4-hour evening rush period). Finally,  $h, w$  correspond to the spatial height and width of the grid, where  $h$  and  $w$  partition the city into spatial regions (e.g., NYC taxi zones). This tensor format cohesively encapsulates ST data, including multiple time intervals, sequences of historical windows, and the spatial layout of the city.

Given a prediction time  $t$  and utilizing historical data spanning up to  $n$  time steps preceding  $t$  (represented as a window of size  $n$ ), the historical inputs  $\mathbf{X}_{t-1}, \dots, \mathbf{X}_{t-n}$  are processed by the BiDepth Encoder. Here, each  $\mathbf{X}_{t-i}$  represents the spatial data (e.g., taxi demands across all zones) at time  $t - i$ . The BiDepth Encoder takes the entire historical window  $\{\mathbf{X}_{t-1}, \dots, \mathbf{X}_{t-n}\}$  as input and learns the spatio-temporal characteristics of the data, focusing on non-stationarity and complex spatial patterns. This results in a set of transformed sequences  $\{\mathbf{X}'_{t-1}, \dots, \mathbf{X}'_{t-n}\}$ , which encapsulate the learned spatial features and patterns. For convenience, we denote the collective transformed historical data as  $\mathbf{X}'_t$ , where  $\mathbf{X}'_t = \{\mathbf{X}'_{t-1}, \dots, \mathbf{X}'_{t-n}\}$ . These transformed

representations are then passed to the TimeSeries Encoder, which captures the temporal dependencies across the entire historical window to produce the final prediction. The comprehensive details of our BiDepth Encoder are presented in Section 2.1.

$$\mathbf{X}'_t = \text{BiDepthEncoder}(\mathbf{X}_{t-1}, \dots, \mathbf{X}_{t-n}). \quad (1)$$

The TimeSeries Encoder offers flexibility in configuration, allowing for either a Convolutional LSTM or a Convolutional Self-Attention mechanism, each providing distinct advantages in modeling temporal dynamics. It predicts the values of  $\mathbf{X}_t$  based on the knowledge of historical spatio-temporal patterns stored in  $\mathbf{X}'_t$ . While the Convolutional LSTM accentuates long-term correlations (e.g., capturing seasonal trends), the Convolutional Self-Attention mechanism allows the model to dynamically identify and weight spatial correlations across the entire sequence. The culmination of this process is the prediction for time  $t$ , denoted as  $\hat{\mathbf{X}}_t$ . The details of the TimeSeries Encoder are introduced in Section 2.2.

$$\hat{\mathbf{X}}_t = \text{TimeSeriesEncoder}(\mathbf{X}'_t). \quad (2)$$

In synergy, the BiDepth Encoder and TimeSeries Encoder craft a robust model for ST data processing, harmoniously merging computational efficiency with nuanced model complexity. The following sections undertake a detailed dissection of each component’s blueprint and functionality.

## 2.1 BiDepth Encoder

The BiDepth Encoder, illustrated in Figure 2, is designed to integrate the capabilities of the two complementary networks: the DeepShallow and ShallowDeep encoders. This encoder serves as the backbone for processing ST data, ensuring a comprehensive and balanced analysis.

Each input,  $\mathbf{X}_{t-i}$  at a specific historical timestamp,  $t-i$ , is processed through both DeepShallow and ShallowDeep networks. In the context of our datasets, this input represents the spatial data at time  $t-i$ , such as the taxi demand across all zones in the TLC dataset or the precipitation measurements across all grid points in the GPM dataset (described in Section 3.1.2). After processing, the BiDepth Encoder combines the outputs of these two encoders. This concatenation step (Szegedy et al, 2015) is pivotal, as it merges insights into a unified representation. The concatenated output is then fed into the TimeSeries Encoder of the BDMNN for subsequent processing and forecasting.

$$\mathbf{X}'_{t-i} = \text{Concat}(\mathbf{X}_{t-i}^{DS}, \mathbf{X}_{t-i}^{SD}), \quad \text{for } i = 1, \dots, n, \quad (3)$$

where  $\mathbf{X}'_{t-i}$  represents the output of the BiDepth Encoder at timestamp  $t-i$ , and  $\mathbf{X}_{t-i}^{DS}$  and  $\mathbf{X}_{t-i}^{SD}$  are the outputs of the DeepShallow and ShallowDeep encoders, respectively, at the same timestamp  $t-i$ . The construction of the network can be summarized in Algorithm 1.

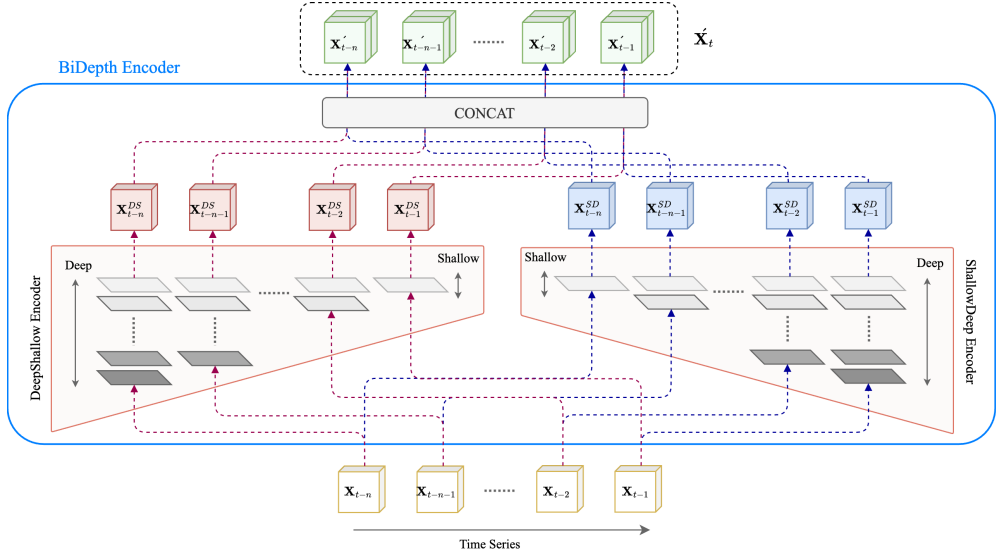


**Fig. 2** Schematic Representation of the BiDepth Encoder Architecture. The BiDepth Encoder consists of two main components: the DeepShallow Encoder and the ShallowDeep Encoder. These encoders analyze time series data differently; the DeepShallow Encoder focuses on deeper layers for earlier time steps and shallower layers for more recent time steps, while the ShallowDeep Encoder does the opposite, emphasizing deeper layers for recent data and shallower layers for older data. Each time component of the series is processed by both encoders, with the results concatenated at the output. The architecture employs a weight-sharing strategy where Convolutional Neural Networks (illustrated as plates) at corresponding depths across the encoders share weights, indicated by the identical shading. This approach facilitates the effective capture of both ST dependencies, enhancing the model’s capability to handle complex ST data.

### 2.1.1 DeepShallow Encoder

The DeepShallow encoder is characterized by two key architectural features: (i) a dynamic adjustment of CNN layer depths as time progresses and (ii) a shared-weight mechanism for layers exhibiting identical depth. We focus on these two features because they are essential for adapting the model to temporal dynamics and improving computational efficiency. These features distinguish our approach from traditional methods that often use fixed-depth layers without weight sharing.

At its core, the DeepShallow encoder processes sequences by channeling each timestamp through a set of CNN layers, as illustrated in Figure 2. Unlike conventional models, these layers are dynamic in depth, changing based on the timestamp’s temporal position. The rationale behind varying the layer depth is to capture the varying complexity of patterns over different time scales. For earlier (older) timestamps, deeper layers can capture complex long-term dependencies, while shallower layers (fewer layers) are sufficient for more recent timestamps where patterns may be simpler or more directly related to the prediction target.

This feature is adjusted by a user-defined function, *depth\_function*, potentially a linear function, that orchestrates the depth transition throughout the sequence. The



---

**Algorithm 1** BiDepth Network Algorithm

---

**Require:** Input tensor  $\mathbf{X} \in \mathbb{R}^{b \times n \times c_{in} \times h \times w}$ , initial maximum depth  $L$ , window size  $n$

**Ensure:** Output tensor  $\hat{\mathbf{X}}_t \in \mathbb{R}^{b \times c_{out} \times h \times w}$

```
1: Initialize:
2:   Convolutional layers  $\{\text{CNN}_d\}_{d=1}^L$  shared across depths
3:   Compute layer decrement  $\delta = \frac{L-1}{n-1}$ 
4:   for  $i = 1$  to  $n$  do
      # DeepShallow (DS) Encoder:
5:     Compute depth for DS:  $D_{(t-i)}^{DS} = \max(1, L - \lfloor (i-1)\delta \rfloor)$ 
6:     for  $d = 1$  to  $D_{(t-i)}^{DS}$  do
7:        $\mathbf{X}_{t-i}^{DS} \leftarrow \text{ReLU}(\text{CNN}_d(\mathbf{X}_{t-i}^{DS}))$ 
8:     end for
      # ShallowDeep (SD) Encoder:
9:     Compute depth for SD:  $D_{(t-i)}^{SD} = \max(1, \lfloor (i-1)\delta \rfloor + 1)$ 
10:    for  $d = 1$  to  $D_{(t-i)}^{SD}$  do
11:       $\mathbf{X}_{t-i}^{SD} \leftarrow \text{ReLU}(\text{CNN}_d(\mathbf{X}_{t-i}^{SD}))$ 
12:    end for
13:  end for
      # Stack outputs over time:
14:   $\mathbf{X}_t^{DS} \leftarrow \text{Stack}(\mathbf{X}_{t-1}^{DS}, \mathbf{X}_{t-2}^{DS}, \dots, \mathbf{X}_{t-n}^{DS})$ 
15:   $\mathbf{X}_t^{SD} \leftarrow \text{Stack}(\mathbf{X}_{t-1}^{SD}, \mathbf{X}_{t-2}^{SD}, \dots, \mathbf{X}_{t-n}^{SD})$ 
      # Concatenate paths along channel dimension:
16:   $\mathbf{X}'_t \leftarrow \text{Concat}(\mathbf{X}_t^{DS}, \mathbf{X}_t^{SD})$ 
      # Apply ConvLSTM or ConvSelfAttention:
17:   $\hat{\mathbf{X}}_t \leftarrow \text{TimeSeriesEncoder}(\mathbf{X}'_t)$ 
18: Return  $\hat{\mathbf{X}}_t$ 
```

---

depth function is mathematically represented as shown in Equation (4), where  $D_{(t-i)}^{DS}$  indicates the number of convolutional layers (i.e., the depth) applied at  $i$  timestamps prior to  $t$ :

$$D_{(t-i)}^{DS} = \max\left(1, L - \left\lfloor \frac{(i-1)(L-1)}{n-1} \right\rfloor\right), \quad \text{for } i = 1, \dots, n. \quad (4)$$

In this function,  $L$  is the initial maximum depth,  $n$  is the window size (number of historical timestamps), and  $i$  indexes the timestamps from the most recent ( $i = 1$ ) to the oldest ( $i = n$ ). The notation  $\lfloor \cdot \rfloor$  indicates rounding to the nearest integer. The depth decreases linearly from  $L$  for the oldest timestamp to 1 for the most recent. Alternative depth functions can be used, but we found the linear function effective in balancing complexity and efficiency.

The number of convolutional layers (LeCun et al, 1998) applied to each timestamp  $t - i$  is given by  $D_{(t-i)}^{DS}$ . Each depth level  $d = 1, \dots, D_{(t-i)}^{DS}$  corresponds to one convolutional layer. To ensure efficiency and prevent overfitting, layers at the same depth level share their weights across all timestamps. This means that if two timestamps use

a layer of depth  $d$ , they apply the same convolutional filters  $W_d$ . As  $D_{(t-i)}^{DS}$  varies over time, certain timestamps may involve fewer layers (shallow configurations) and others more layers (deeper configurations), but layers at the same depth index  $d$  always use the same set of shared weights  $W_d$ .

Formally, given the shared weights  $W_d$  for each depth level  $d$ , the output  $\mathbf{X}_{t-i}^{DS}$  for timestamp  $t - i$  is:

$$\mathbf{X}_{t-i}^{DS} = \text{CNN}_{D_{(t-i)}^{DS}} \left( \mathbf{X}_{t-i}; \{W_d\}_{d=1}^{D_{(t-i)}^{DS}} \right), \quad \text{for } i = 1, \dots, n, \quad (5)$$

where  $\text{CNN}_{D_{(t-i)}^{DS}}(\cdot)$  indicates applying  $D_{(t-i)}^{DS}$  convolutional layers in sequence, each layer identified by a distinct depth index  $d$ . The set  $\{W_d\}_{d=1}^{D_{(t-i)}^{DS}}$  denotes the weights for all layers up to the current depth. Layers with the same depth index  $d$  use the same weights  $W_d$  at every timestamp where that depth is employed, ensuring consistent feature extraction across different temporal contexts. By sharing weights among layers of the same depth, the model reduces the total number of parameters and learns generalized features that remain effective across varying time steps.

### 2.1.2 ShallowDeep Encoder

The ShallowDeep encoder adopts an inverse strategy compared to the DeepShallow encoder. Instead of decreasing layer depth over time, it increases the number of convolutional layers for more recent timestamps, focusing on short-term, complex patterns. This approach allows for more detailed modeling of recent data, where abrupt changes and localized events may require a higher number of convolutional layers. The depth function for the ShallowDeep encoder is defined as:

$$D_{(t-i)}^{SD} = \max \left( 1, \left\lfloor \frac{(i-1)(L-1)}{n-1} \right\rfloor + 1 \right), \quad \text{for } i = 1, \dots, n, \quad (6)$$

where  $D_{(t-i)}^{SD}$  specifies how many convolutional layers are applied at timestamp  $t - i$ . The depth increases from 1 for the oldest timestamp to  $L$  for the most recent, reflecting the need for deeper modeling of current short-term dependencies. Similar to the DeepShallow encoder, the ShallowDeep encoder employs a weight-sharing mechanism where all layers at the same depth index share a common set of weights  $W_d$ . Given the shared weights for each depth level, the output  $\mathbf{X}_{t-i}^{SD}$  is:

$$\mathbf{X}_{t-i}^{SD} = \text{CNN}_{D_{(t-i)}^{SD}} \left( \mathbf{X}_{t-i}; \{W_d\}_{d=1}^{D_{(t-i)}^{SD}} \right), \quad \text{for } i = 1, \dots, n. \quad (7)$$

In this operation,  $\text{CNN}_{D_{(t-i)}^{SD}}(\cdot)$  applies  $D_{(t-i)}^{SD}$  convolutional layers in sequence, each identified by a depth index  $d$ . Layers sharing the same depth index use the same weights  $W_d$  across all timestamps, ensuring consistent feature extraction and efficient parameter utilization.

## 2.2 TimeSeries Encoder

The TimeSeries Encoder is responsible for modeling the temporal dependencies in the transformed spatial representations  $\mathbf{X}'_t$  produced by the BiDepth Encoder. It takes

$\mathbf{X}'_t \in \mathbb{R}^{b \times n \times c \times h \times w}$  as input, where the dimensions  $b, n, c, h, w$  follow the definitions provided in the BiDepth Encoder section.

While our framework can employ various temporal modeling approaches, such as a Convolutional LSTM (Shi et al, 2015), our primary contribution lies in the development of a Convolutional Transformer-based TimeSeries Encoder. This design leverages CASC to capture temporal dependencies without discarding spatial information. The CASC developed in our work addresses the challenge of effectively retaining spatial information during the application of attention mechanisms (Guo et al, 2019). Our experimental results (see Section 3.3) indicate that this Convolutional Transformer approach outperforms the ConvLSTM baseline, particularly in handling complex ST correlations and multi-scale dynamics.

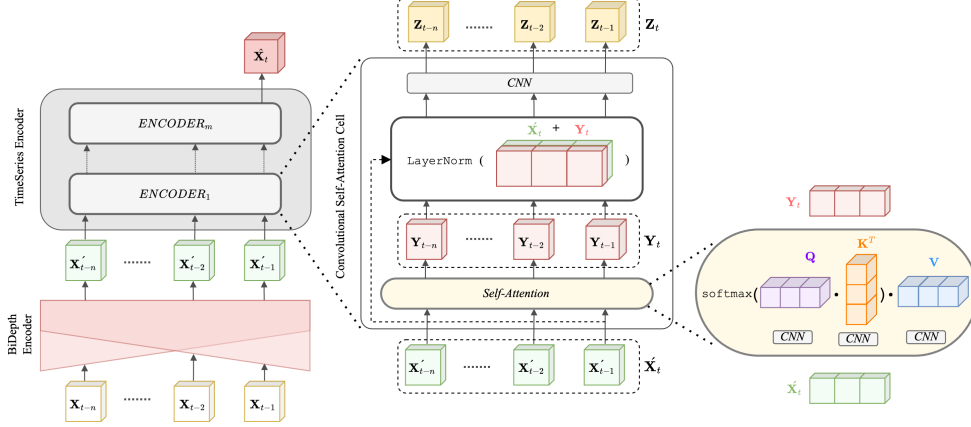


**Fig. 3** Illustration of the Convolutional Self-Attention Cell. The cell’s internal workflow is displayed, emphasizing the processing of the input tensor through the Self-Attention layer. This layer employs 2D convolutional layers to generate the query, key, and value tensors for calculating attention weights. Subsequent to this, the attention mechanism modifies the value tensor, yielding an output that is conscious of other timestamps. The final output merges the input tensor with these attention-informed tensors, passing through layer normalization and an additional 2D convolution layer. This process exemplifies our model’s ability to seamlessly incorporate the attention mechanism while safeguarding the input data’s spatial structure.

The CSAC, as illustrated in Figure 3, extends the self-attention mechanism by preserving spatial structures through convolutional operations. Let  $\mathbf{X}'_t \in \mathbb{R}^{b \times n \times c \times h \times w}$  be the input sequence of transformed spatial features over  $n$  time steps. We employ three separate convolutional operations to generate query ( $\mathbf{Q}$ ), key ( $\mathbf{K}$ ), and value ( $\mathbf{V}$ ) tensors from  $\mathbf{X}'_t$ . Formally, we define:

$$\mathbf{Q} = \text{CNN}(\mathbf{X}'_t; W_Q), \quad \mathbf{K} = \text{CNN}(\mathbf{X}'_t; W_K), \quad \mathbf{V} = \text{CNN}(\mathbf{X}'_t; W_V), \quad (8)$$

where  $\mathbf{Q}$ ,  $\mathbf{K}$ , and  $\mathbf{V}$  represent convolutional mappings (LeCun et al, 1998), each parameterized by its own weights ( $W_Q, W_K, W_V$ ). These convolutions retain the spatial dimensions ( $h, w$ ), ensuring that spatial relationships are not lost. After reshaping

$\mathbf{Q}$  and  $\mathbf{K}$  for the attention computation, the attention scores  $\mathbf{A}$  are obtained via a softmax operation applied to  $\mathbf{QK}^T$  (where  $\mathbf{K}^T$  denotes the transpose of  $\mathbf{K}$ ):

$$\mathbf{A} = \text{softmax}(\mathbf{QK}^T), \quad (9)$$

$\mathbf{A} \in \mathbb{R}^{b \times n \times n}$  represents the temporal attention weights, indicating how each time step in the sequence attends to every other time step. Applying these attention weights to  $\mathbf{V}$  yields the attention-informed output  $\mathbf{Y}_t$ :

$$\mathbf{Y}_t = \mathbf{AV}, \quad (10)$$

$\mathbf{Y}_t$  shares the same shape as  $\mathbf{X}'_t$ , i.e.,  $\mathbf{Y}_t \in \mathbb{R}^{b \times n \times c \times h \times w}$ , ensuring that the output remains spatially coherent. Here,  $\mathbf{A}$  encodes temporal correlations between different time steps, and by applying  $\mathbf{A}$  to  $\mathbf{V}$ , we produce  $\mathbf{Y}_t$  that emphasizes relevant temporal patterns across the entire sequence.

In the final integration step, we concatenate (Szegedy et al, 2015) the original input  $\mathbf{X}'_t$  with the attention-informed output  $\mathbf{Y}_t$ , forming  $\text{concat}(\mathbf{X}'_t, \mathbf{Y}_t)$ . This concatenated tensor is then normalized using Layer Normalization and passed through an additional 2D convolutional layer:

$$\mathbf{Y}_t^{\text{norm}} = \text{LayerNorm}(\text{Concat}(\mathbf{X}'_t, \mathbf{Y}_t)), \quad (11)$$

$$\mathbf{Z}_t = \text{CNN}(\mathbf{Y}_t^{\text{norm}}; W_O), \quad (12)$$

where  $\mathbf{Z}_t \in \mathbb{R}^{b \times n \times c \times h \times w}$  represents the final output of the TimeSeries Encoder, combining the original input features with the attention-derived insights.  $\text{CNN}(\cdot; W_O)$  is another convolutional operation (LeCun et al, 1998) with its own learnable weights  $W_O$ , ensuring a flexible representation that can adapt to various ST complexities.

The Convolutional Transformer-based TimeSeries Encoder integrates convolutional operations within the self-attention mechanism to preserve spatial integrity, adaptively focus on temporal dependencies, and produce a refined output  $\mathbf{Z}_t$ . This approach provides a more expressive modeling framework than the ConvLSTM, as evidenced by our empirical evaluations, and can be extended to multi-headed or multi-layered structures for capturing increasingly complex spatial and temporal relationships.

### 2.3 Evaluation Metrics

Our primary quantitative measures for model assessment were the Mean Squared Error (MSE) and the Mean Absolute Error (MAE). Both metrics are widely used in regression tasks, offering complementary insights into the model’s predictive performance (Pan et al, 2024). The MSE is defined as:

$$MSE = \frac{1}{s} \sum_{i=1}^s \frac{1}{h \times w} \sum_{j=1}^h \sum_{k=1}^w (X_{i,j,k} - \hat{X}_{i,j,k})^2, \quad (13)$$

where  $X_{i,j,k}$  and  $\hat{X}_{i,j,k}$  denote the true and predicted values at spatial coordinates  $(j, k)$  for the  $i$ -th sample, and  $s, h, w$  represent the number of samples, and the spatial

dimensions of the prediction respectively. MSE evaluates the average squared error and heavily penalizes larger deviations. This makes it valuable for identifying when the model significantly under- or overestimates the target, thus providing a sensitive gauge of model stability and performance.

MAE measures the average absolute error in the same units as the predicted quantity, offering a direct and intuitive interpretation of the model’s typical error magnitude. This linear treatment of errors makes MAE particularly useful for interpreting spatial distributions of prediction errors. For instance, an MAE of 4 for a zone in TLC data can be directly understood as being off by about 4 passengers on average. Such interpretability aids in practical decision-making and in understanding where and by how much the model tends to mispredict. The MAE is defined as:

$$MAE = \frac{1}{s} \sum_{i=1}^s \frac{1}{h \times w} \sum_{j=1}^h \sum_{k=1}^w |X_{i,j,k} - \hat{X}_{i,j,k}|. \quad (14)$$

## 2.4 Model Hyperparameter Tuning

The performance of the BDMNN depends on several hyperparameters that control the architecture and training process. Key hyperparameters include the initial depth of the convolutional layers, the window size (number of historical timestamps used), the choice of activation functions, learning rate, batch size, and the number of filters in the convolutional layers. Among these, the initial depth of the convolutional layers ( $L$ ) in the BiDepth Encoder is a significant hyperparameter that directly affects the model’s capacity to capture both historical and recent trends in the data. The initial depth ( $L$ ) determines the maximum number of convolutional layers through which the data passes at each timestamp, as governed by the depth functions defined in Equations (4) and (6).

Our analysis has shown that increasing  $L$  can lead to improved model performance up to a certain point. Specifically, as the depth increases, the MSE on the validation set decreases, indicating better predictive accuracy. However, this comes at the cost of increased computational complexity and longer training times. There is a trade-off between model depth, predictive performance, and computational cost. An optimal depth exists where the MSE is minimized without incurring unnecessary computational overhead. Selecting this optimal depth requires balancing the benefits of increased model capacity with the practical considerations of training time and resource availability.

In our experiments, detailed in Section 3.4, we empirically evaluate the impact of the initial depth on the BDMNN’s performance using the TLC data. The results corroborate the conceptual understanding, showing that beyond a certain depth, further increases do not significantly improve MSE but do increase training time.

## 3 Case Studies

To demonstrate the effectiveness of the proposed BDMNN, we conducted two case studies with two different ST datasets: the NYC TLC data and the GPM datasets. By leveraging these datasets, we aim to validate our model’s versatility across diverse

complexities and applicative domains. The NYC TLC data preprocessing details can be found in Subsection 3.1. Table 2 summarizes the key ST characteristics of the two datasets, highlighting high dimensionality, ST correlation, and evolving non-stationary patterns.

**Table 2** ST Characteristics of the Datasets

ST Characteristic	TLC Dataset	GPM Dataset
<b>High Dimensionality</b>	<ul style="list-style-type: none"> <li>• Over 200 taxi zones</li> <li>• 15-min intervals</li> <li>• Over three years</li> </ul>	<ul style="list-style-type: none"> <li>• Spatial resolution of 0.1°</li> <li>• Covering continental US</li> <li>• 30-min precipitation data</li> <li>• Over 6 years</li> </ul>
<b>Complex ST Correlations</b>	<ul style="list-style-type: none"> <li>• Taxi demand in one zone impacted by adjacent zones and recent trends</li> </ul>	<ul style="list-style-type: none"> <li>• Precipitation at a grid affected by neighboring grids and temporal evolution of weather systems</li> </ul>
<b>Non-Stationary Patterns</b>	<ul style="list-style-type: none"> <li>• Short-term spikes during rush hours or disruptions</li> <li>• Long-term seasonal trends like higher demand during holidays or summer</li> </ul>	<ul style="list-style-type: none"> <li>• Short-term events like sudden storms or flash floods</li> <li>• Long-term seasonal trends such as monsoon rainfall increases</li> </ul>

## 3.1 Data Preprocessing

### 3.1.1 TLC Data

Originating from the NYC TLC, the TLC Trip Record Data offers an exhaustive snapshot of taxi trips in New York City (NYC Taxi and Limousine Commission, 2024). The data, sourced from authorized technology providers under the Taxicab & Livery Passenger Enhancement Programs (TPEP/LPEP), encompasses attributes such as pick-up and drop-off dates/times, locations, trip distances, itemized fares, rate types, payment types, and driver-reported passenger counts. Despite TLC’s continuous reviews to ensure completeness and accuracy, the published data may not encapsulate all trips dispatched by TLC-licensed bases, highlighting the vast and complex nature of urban transport data. This dataset spans from 2009 to 2023, offering a comprehensive temporal landscape to evaluate the BDMNN. However, leveraging this dataset for our BDMNN required transforming it into a format that captures both ST dynamics. Consequently, our primary aim was to sculpt a ST tensor representing the taxi traffic patterns for a day based on the data from the preceding day.

The dataset was divided into a training set that includes data from 2021 and 2022, and a testing and validation set that contains data from 2023. By allocating older data for training and more recent data for validation and testing, we simulate a realistic forecasting scenario where the model predicts future patterns without access to future information during training. This chronological division reduces the risk of the model overfitting to temporal trends observed in future data, thereby ensuring a more unbiased and reliable model assessment. For a rigorous model evaluation, we split the 2023 data into two: the initial half (January to March) served as the validation

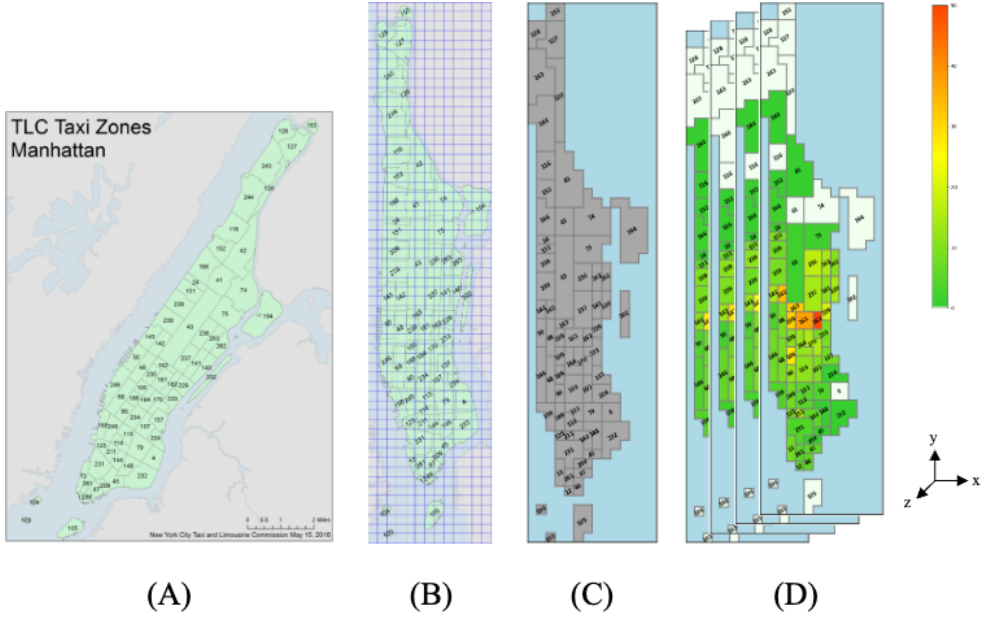


**Fig. 4** Sequential depiction of the New York City taxi zone processing. (A) Original TLC map marking various taxi zones in NYC. (B) After rotation for optimal tensor representation, the map showcases a grid layout matched to the smallest taxi zone’s dimensions. This assures a uniform and detailed citywide spatial segmentation. (C) The post-pixelation view where each grid cell’s value is ascertained using a max pooling approach, correlating it with the dominant zone. (D) The 3D tensor visualization conveys the transformation of pickup data into a ST structure, where  $x$  and  $y$  dimensions are spatial coordinates across NYC, and the  $z$ -dimension signifies time. Each tensor cell value indicates the passenger pickups in a grid segment during a specific 15-minute window, converting the city map into a succinct ST representation.

set for model parameter tuning and optimization, while the latter half (April to May) functioned as the testing set.

Concentrating on essential features of the dataset, such as pickup and drop-off times, locations, and passenger count, we focused on two critical periods to capture the pulse of urban transportation: the evening rush hour from 4 PM to 6 PM and the morning hours from 6 AM to 10 AM. The pickup data during the evening rush hour was aggregated into 15-minute intervals, crafting a temporal sequence of passenger pickups. Concurrently, we transformed the morning drop-off data similarly, providing another perspective on taxi service distribution and density.

Addressing the spatial dimension was challenging due to the dataset’s discrete location identifiers. Our remedy was the provided NYC taxi zone map (Figure 4A-C). The NYC taxi dataset divides the city into approximately 200 zones. We identified the smallest zone (i.e., the one with the least area) and used its dimensions to define a uniform grid overlaying the entire city. Each grid cell’s zone identity is determined by the zone covering the largest fraction of that cell’s area, effectively “assigning precedence” to the dominant zone within that cell. This approach, inspired by the ‘max pooling’ concept in image processing, creates a grid-based representation of zones.

We validated the spatial representation accuracy by comparing the actual area proportions of Manhattan zones to their "pixelated" (grid-based) counterparts. The average error rate between these two representations, weighted by the demand (average passenger count per location for each 15-minute interval), was found to be approximately 0.1. To calculate this, we first determined the area proportion of each zone in Manhattan based on the actual area and the grids, then computed the absolute difference between these two proportions for each zone. These differences were weighted by the respective location demand before averaging. For context, the mean demand per zone per 15-minute interval in our dataset is around 50 passengers, with a standard deviation of about 15 passengers. An average misallocation of 0.1 passengers implies that the spatial discretization introduced by the grid mapping minimally affects the overall demand distribution. The range of weighted errors varied, with a minimum of 0.00019, a maximum of 1.11689, and a standard deviation of 0.17495, reflecting the distribution of demand across zones. Since this error pertains to spatial relationships and typically occurs between neighboring zones, the impact of such misallocation on modeling performance is minimal.

Following this spatial structuring, we integrated the temporally formatted pickup and drop-off data, converting our 2D grid into a 3D tensor. This tensor combined two spatial dimensions and a third temporal dimension, marked by successive 15-minute intervals. Within this tensor, each cell value conveys the passenger pickups for a specific zone during a designated time slot, crafting a dynamic traffic heatmap of New York City (Figure 4D). In this heatmap, colors represent the intensity of demand, with warmer colors typically indicating higher passenger counts and cooler colors indicating lower counts. We then focused on Manhattan, presenting a time-sensitive, spatially granular depiction of passenger demands in this area.

### 3.1.2 GPM Data

We utilized the GPM dataset described by [Ehsani et al \(2022\)](#) in their NowCasting research. This dataset spans six years (2015-2020) and consists of the Global Precipitation Measurement (GPM) Integrated Multi-satellite Retrievals for GPM (IMERG) early run products ([Huffman et al, 2020](#)). It offers half-hourly precipitation maps at a spatial resolution of  $0.1^\circ$  across the Continental United States (CONUS).

The dataset was divided into training (85%), validation (5%), and testing (10%) sets based on chronological order, with the most recent 10% reserved for testing. This approach ensures the model is trained on past precipitation patterns and evaluated on future periods, mirroring real-world forecasting conditions. Throughout the training period, the model consistently uses a 24-hour historical window to predict the subsequent 4 hours of precipitation, maintaining a uniform training strategy over the entire training dataset.

## 3.2 Computational Setup

All experiments were conducted on NVIDIA A100 GPUs to ensure consistency across different datasets. The BDMNN and all baseline models were implemented using PyTorch. We employed hyperparameter tuning for all experiments to optimize model



performance. Key hyperparameters included a learning rate of 0.005 for the AdamW optimizer and the use of MSE as the loss function. We also implemented early stopping with patience to prevent overfitting and improve training efficiency. The training time varied depending on the dataset, with an average of approximately 320 minutes for the GPM data and 8 minutes for the TLC data. To ensure reproducibility and assess model stability, we ran each model configuration with different random seeds at least 5 times, reporting the mean performance.

### 3.3 Results

The evaluation utilized the MSE loss mentioned in Section 2.3. This section aims to delve into the performance of the BDMNN and its variants, providing insights into the model’s capabilities across the datasets.

#### 3.3.1 TLC Trip Record Prediction

For the TLC data, Table 3 showcases the performance of different models on the TLC Data, emphasizing the improvements realized by incorporating the BiDepthNet structure.

Model	Model Complexity*	MSE	Improvements (%)
ARIMA (Dubey et al, 2021)	-	6.455	-
SARIMA (Dubey et al, 2021)	-	5.517	-
U-Net (Ronneberger et al, 2015)	2,000	3.021	-
CNN-RNN (Lu et al, 2020)	2,400	2.305	-
ViViT (Arnab et al, 2021)	460	1.831	-
ConvLSTM (Shi et al, 2015)	560	1.652	-
+ DeepShallow	600	1.515	+ 9.87
+ ShallowDeep	600	1.500	+ 9.19
+ BiDepthNet	660	1.479	+ 10.47
ConvSelfAttention	350	1.621	-
+ DeepShallow	380	1.503	+ 7.27
+ ShallowDeep	380	1.580	+ 2.51
+ BiDepthNet	440	<b>1.428</b>	+ 11.89

**Table 3** Performance comparison and model complexity of BiDepth versus Benchmarks on TLC Data. The performance depicted is based on MSE loss. The model parameters are presented in thousands. Models with modifications, such as “+ DeepShallow,” “+ ShallowDeep,” and “+ BiDepthNet,” denote enhancements made to the foundational models. The reported improvements correspond to the percentage increase in performance (decrease in MSE) achieved by incorporating the introduced encoders (BiDepth, DeepShallow) into the base TimeSeries Encoders (e.g., ConvLSTM, ConvSelfAttention).

\* Model complexity is assessed based on the number of parameters in thousands (K). For instance, U-Net has approximately 2 million parameters.

The results highlight the effectiveness of integrating DeepShallow, ShallowDeep, and BiDepthNet into base models like ConvLSTM and ConvTransformer. Notably, enhancements with DeepShallow and ShallowDeep architectures lead to significant improvements. For instance, the ConvLSTM model’s MSE decreases from 1.652

to 1.515 with DeepShallow, and further to 1.500 with ShallowDeep. The ConvLSTM model enhanced with BiDepthNet achieves an MSE of 1.479, while the ConvTransformer combined with BiDepthNet records the lowest MSE of 1.428.

These improvements underscore the proposed method’s ability to more effectively exploit spatio-temporal structures. By dynamically adjusting network depth to balance short-term fluctuations and long-term trends, and preserving spatial correlations, the BDMNN captures the inherent complexity of ST data better than baseline models. This synergy translates into more accurate predictions across diverse scenarios.

### *Spatial MAE Analysis*

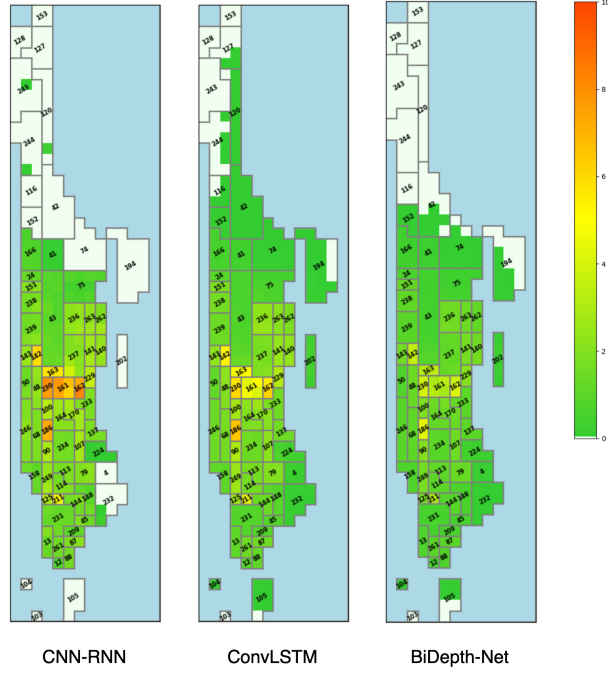


**Fig. 5** Spatial MAE distribution over Manhattan for different models, based on the average MAE between prediction and the label across the whole test set and all time-stamps. The variance in heatmaps reveals prediction discrepancies across taxi zones. Distinctly, the BDMNN model manifests consistently minimal errors throughout most zones, emphasizing its superior ST predictive capability.

To better understand the spatial performance of the BDMNN relative to other benchmark models, we produced an MAE heatmap for the Manhattan region. This heatmap reflects the spatial distribution of prediction errors, averaged across the entire test set and all time-stamps, providing granular insight into where models succeed or struggle. As illustrated in Figure 5, while each model exhibits areas of strength, the BDMNN consistently achieves notably lower error rates throughout Manhattan. Such a spatially resolved analysis demonstrates that the BDMNN not only excels in aggregate metrics like MSE but also delivers consistently lower per-zone errors.

This spatial adaptability suggests that the BDMNN is better aligned with local ST dynamics, leading to more reliable predictions in diverse urban contexts.

### 3.3.2 GPM Forecasting

The results for the GPM dataset are presented in Table 4. Consistent with the findings from the TLC dataset, the BiDepth variants outperformed the baseline models, showing over a 14.58% improvement when added to the ConvSelfAttention model and a 17.92% improvement when compared to the widely used ConvLSTM baseline. This consistent superiority across diverse datasets highlights the robustness and adaptability of the BDMNN, indicating its potential for a wide range of ST forecasting applications. In the context of weather forecasting, improvements in MSE can yield substantial real-world benefits—enhancing resource planning, risk mitigation, and operational efficiency. The demonstrated improvements underscore the BDMNN’s capacity to more effectively capture complex spatio-temporal correlations, thus providing more reliable predictions in demanding scenarios.

Model	Model Complexity*	MSE	Improvements (%)
ARIMA (Dubey et al, 2021)	-	12.907	-
SARIMA (Dubey et al, 2021)	-	11.088	-
U-Net (Ronneberger et al, 2015)	2,000	3.920	-
CNN-RNN (Lu et al, 2020)	3,500	5.112	-
ViViT (Arnab et al, 2021)	4,200	3.112	-
ConvLSTM (Shi et al, 2015)	1,520	3.071	-
+ DeepShallow	1,600	2.779	+ 9.48
+ ShallowDeep	1,600	2.951	+ 3.87
+ BiDepthNet	1,680	2.861	+ 6.84
ConvSelfAttention	2,100	2.951	-
+ DeepShallow	2,180	2.863	+ 2.95
+ ShallowDeep	2,180	2.861	+ 3.02
+ BiDepthNet	2,260	<b>2.520</b>	+ 14.58

**Table 4** Performance comparison and parameter sizes of BiDepth versus Benchmarks on GPM Data. The model parameters are presented in thousands. The performance depicted is based on MSE loss. Models with modifications such as ”+ DeepShallow”, ”+ ShallowDeep”, and ”+ BiDepthNet” indicate enhancements made to the base models. The reported improvements reflect the percentage increase in performance (reduction in MSE) when incorporating the introduced encoders (BiDepth, DeepShallow) into the base TimeSeries Encoders (e.g., ConvLSTM, ConvSelfAttention).

\* Model complexity is assessed based on the number of parameters in thousands (K). For instance, U-Net has approximately 2 million parameters.

### 3.4 Impact of Initial Depth in the BDMNN

The initial depth in our BDMNN, a significant hyperparameter, determines the extent of depth possibly needed to capture both historical and recent trends. To understand this relationship, we varied the initial depth and monitored its influence on the MSE in the Validation set as well as the training time for the TLC data.

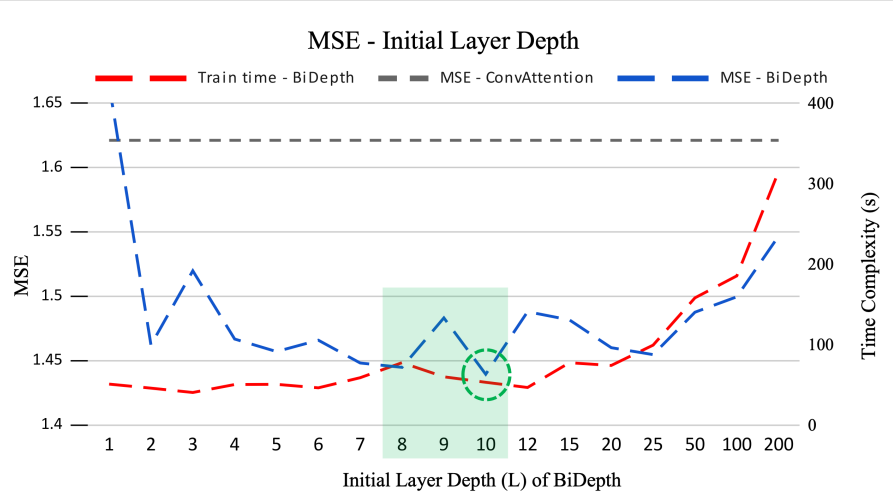


**Fig. 6** A clear trend is observed, with MSE decreasing as depth increases up to a certain point, after which performance stabilizes while training time continues to rise. The left axis illustrates the MSE for both ConvAttention and BiDepth, while the right axis depicts the training time in seconds. The highlighted area and circled values are the recommended  $L$  based on our analysis. This highlights the trade-off between enhanced performance and increased computational cost as model depth grows.

Figure 6 demonstrates that as the initial depth amplifies, the MSE correspondingly drops, signaling improved model performance. However, there’s a discernible inflection point beyond which additional depth no longer enhances accuracy, however it increases the training time. This optimal juncture provides a glimpse into the data’s temporal nature, suggesting a balance between recent and historical data.

## 4 Conclusion and Future Work

In this study, we introduced the BDMNN, a novel architecture adept at capturing intricate temporal dependencies by dynamically adjusting its depth. Our experiments spanned two distinct datasets, providing a comprehensive evaluation of the proposed model. The BDMNN network consistently outperformed benchmark models across diverse datasets, testifying to its robustness and adaptability. Incorporating attention mechanisms further enhanced the model’s predictive prowess, emphasizing the significance of context-aware temporal learning. An exploration into the model’s depth revealed a balance between immediate and historical data, suggesting an optimal temporal granularity for prediction tasks. Spatial analyses highlighted the BDMNN’s capacity to uniformly capture ST patterns, an attribute crucial for applications in dynamic urban environments.

The ConvSelfAttention mechanism demonstrated superior performance compared to ConvLSTM and enabled parallel tensor processing, but it exhibits limitations related to model size scaling. Unlike ConvLSTM, whose parameter count is primarily defined by hyperparameters and not directly by input size, ConvSelfAttention’s parameter size scales with the spatial dimensions of the input. For smaller spatial

inputs such as the TLC data (14x58 pixels), the ConvSelfAttention model required fewer parameters than ConvLSTM, as shown in Table 3. However, for larger inputs like the GPM data (256x512 pixels), the ConvSelfAttention model’s parameters expanded significantly due to its dependency on input size. We adjusted the ConvLSTM size to be comparable with the ConvSelfAttention for fair comparison, as detailed in Table 4. This input-size dependency of ConvSelfAttention increases computational costs, training time, and memory usage, posing scalability challenges in high-resolution datasets. Future research could address these limitations by exploring more efficient attention mechanisms, adaptive architectures, or model compression techniques to retain the advantages of attention-based models without incurring such computational burdens.

Looking ahead, the versatility of the BDMNN architecture positions it as a promising candidate for broader applications, transcending the domains we explored. Its inherent flexibility opens avenues for further refinements, potentially tailoring it to more specific prediction challenges. Building on the promising results of the BDMNN, several directions can be considered for future investigations. (i) Developing a methodology that allows the model to autonomously adjust the depth of its CNN layers for each input sequence would be a significant advancement. (ii) The current architecture can be extended with multi-modal inputs. Incorporating additional data streams, like weather patterns or event data, could refine predictions in urban contexts where external factors influence traffic or weather patterns. (iii) Exploring the potential of the BDMNN in transfer learning scenarios can be beneficial. Pre-training the model on a larger dataset and fine-tuning on specific tasks or regions may enhance its generalization capabilities.

## References

- Aburas MM, Ahamad MSS, Omar NQ (2019) Spatio-temporal simulation and prediction of land-use change using conventional and machine learning models: A review. *Environmental monitoring and assessment* 191:1–28
- Adhikari R, Agrawal RK (2013) An introductory study on time series modeling and forecasting. arXiv preprint arXiv:13026613
- Ali A, Zhu Y, Zakarya M (2022) Exploiting dynamic spatio-temporal graph convolutional neural networks for citywide traffic flows prediction. *Neural networks* 145:233–247
- Amato F, Guignard F, Robert S, et al (2020) A novel framework for spatio-temporal prediction of environmental data using deep learning. *Scientific reports* 10(1):22243
- Arnab A, Dehghani M, Heigold G, et al (2021) Vivit: A video vision transformer. In: *Proceedings of the IEEE/CVF international conference on computer vision*, pp 6836–6846
- Arroyo J, Maté C (2009) Forecasting histogram time series with k-nearest neighbours methods. *International Journal of Forecasting* 25(1):192–207

- Casallas A, Jiménez-Saenz C, Torres V, et al (2022) Design of a forest fire early alert system through a deep 3d-cnn structure and a wrf-cnn bias correction. *Sensors* 22(22):8790
- Cressie N, Wikle CK (2011) *Statistics for spatio-temporal data*. John Wiley & Sons
- Deng D, Shahabi C, Demiryurek U, et al (2016) Latent space model for road networks to predict time-varying traffic. In: *Proceedings of the 22nd ACM SIGKDD international conference on knowledge discovery and data mining*, pp 1525–1534
- Dubey AK, Kumar A, García-Díaz V, et al (2021) Study and analysis of sarima and lstm in forecasting time series data. *Sustainable Energy Technologies and Assessments* 47:101474
- Ehsani MR, Zarei A, Gupta HV, et al (2022) Nowcasting-nets: Representation learning to mitigate latency gap of satellite precipitation products using convolutional and recurrent neural networks. *IEEE Transactions on Geoscience and Remote Sensing* 60:1–21
- Ehsani S, Liu J (2024) From the depths to the surface: Navigating spatial temporal data with deepshallow network. In: *51th International Conference on Computers & Industrial Engineering (CIE51)*
- Ehsani S, Sergeeva E, Murdy W, et al (2024) Predicting the skies: A novel model for flight-level passenger traffic forecasting. *arXiv preprint arXiv:240103397*
- Feng X, Ling X, Zheng H, et al (2018) Adaptive multi-kernel svm with spatial-temporal correlation for short-term traffic flow prediction. *IEEE Transactions on Intelligent Transportation Systems* 20(6):2001–2013
- Geng X, Li Y, Wang L, et al (2019) Spatiotemporal multi-graph convolution network for ride-hailing demand forecasting. In: *Proceedings of the AAAI conference on artificial intelligence*, pp 3656–3663
- Guo S, Lin Y, Feng N, et al (2019) Attention based spatial-temporal graph convolutional networks for traffic flow forecasting. In: *Proceedings of the AAAI conference on artificial intelligence*, pp 922–929
- He Z, Chow CY, Zhang JD (2019) Stcnn: A spatio-temporal convolutional neural network for long-term traffic prediction. In: *2019 20th IEEE International Conference on Mobile Data Management (MDM)*, IEEE, pp 226–233
- Hochreiter S, Schmidhuber J (1997) Long short-term memory. *Neural computation* 9(8):1735–1780
- Huffman GJ, Bolvin DT, Braithwaite D, et al (2020) Integrated multi-satellite retrievals for the global precipitation measurement (gpm) mission (IMERG). *Satellite*

precipitation measurement: Volume 1 pp 343–353

- Lai G, Chang WC, Yang Y, et al (2018) Modeling long-and short-term temporal patterns with deep neural networks. In: The 41st international ACM SIGIR conference on research & development in information retrieval, pp 95–104
- LeCun Y, Bottou L, Bengio Y, et al (1998) Gradient-based learning applied to document recognition. *Proceedings of the IEEE* 86(11):2278–2324
- LeCun Y, Bengio Y, Hinton G (2015) Deep learning. *nature* 521(7553):436–444
- Li X, Pan G, Wu Z, et al (2012) Prediction of urban human mobility using large-scale taxi traces and its applications. *Frontiers of computer science* 6:111–121
- Li Y, Yu R, Shahabi C, et al (2017) Diffusion convolutional recurrent neural network: Data-driven traffic forecasting. *arXiv preprint arXiv:170701926*
- Ling S, Yu Z, Cao S, et al (2023) Sthan: Transportation demand forecasting with compound spatio-temporal relationships. *ACM Transactions on Knowledge Discovery from Data* 17(4):1–23
- Lu W, Li J, Li Y, et al (2020) A cnn-lstm-based model to forecast stock prices. *Complexity* 2020(1):6622927
- Marchang N, Tripathi R (2020) Knn-st: Exploiting spatio-temporal correlation for missing data inference in environmental crowd sensing. *IEEE Sensors Journal* 21(3):3429–3436
- Moreira-Matias L, Gama J, Ferreira M, et al (2013) Predicting taxi–passenger demand using streaming data. *IEEE Transactions on Intelligent Transportation Systems* 14(3):1393–1402
- NYC Taxi and Limousine Commission (2024) Tlc trip record data. URL <https://www.nyc.gov/site/tlc/about/tlc-trip-record-data.page>, accessed on November 30, 2024
- Pan F, Zhang Y, Liu J, et al (2024) Reliability modeling for perception systems in autonomous vehicles: A recursive event-triggering point process approach. *Transportation Research Part C: Emerging Technologies* 169:104868
- Ronneberger O, Fischer P, Brox T (2015) U-net: Convolutional networks for biomedical image segmentation. In: *Medical image computing and computer-assisted intervention—MICCAI 2015: 18th international conference, Munich, Germany, October 5-9, 2015, proceedings, part III* 18, Springer, pp 234–241
- Salekin MS, Zamzmi G, Goldgof D, et al (2021) Multimodal spatio-temporal deep learning approach for neonatal postoperative pain assessment. *Computers in biology and medicine* 129:104150

- Shekhar S, Williams BM (2007) Adaptive seasonal time series models for forecasting short-term traffic flow. *Transportation Research Record* 2024(1):116–125
- Shi X, Yeung DY (2018) Machine learning for spatiotemporal sequence forecasting: A survey. *arXiv preprint arXiv:180806865*
- Shi X, Chen Z, Wang H, et al (2015) Convolutional lstm network: A machine learning approach for precipitation nowcasting. *Advances in neural information processing systems* 28
- Song J, Zhao C, Lin T, et al (2019) Spatio-temporal patterns of traffic-related air pollutant emissions in different urban functional zones estimated by real-time video and deep learning technique. *Journal of Cleaner Production* 238:117881
- Szegedy C, Liu W, Jia Y, et al (2015) Going deeper with convolutions. In: *Proceedings of the IEEE conference on computer vision and pattern recognition*, pp 1–9
- Tong Y, CHEN Y, ZHOU Z, et al (2017) The simpler the better: A unified approach to predicting original taxi demands on large-scale online platforms.(2017). In: *Proceedings of the 23rd ACM SIGKDD International Conference on Knowledge Discovery and Data Mining*, Halifax, Canada, pp 13–17
- Wang S, Cao J, Philip SY (2020) Deep learning for spatio-temporal data mining: A survey. *IEEE transactions on knowledge and data engineering* 34(8):3681–3700
- Xia S, Zhang Y, Lansey K, et al (2025) Penalized spatial-temporal sensor fusion for detecting and localizing bursts in water distribution systems. *Information Fusion* p 102912
- Xian X, Ye H, Wang X, et al (2021) Spatiotemporal modeling and real-time prediction of origin-destination traffic demand. *Technometrics* 63(1):77–89
- Yang H, Pan F, Tong D, et al (2024) Measurement error-tolerant poisson regression for valley fever incidence prediction. *IISE Transactions on Healthcare Systems Engineering* 14(4):305–317
- Yao H, Wu F, Ke J, et al (2018) Deep multi-view spatial-temporal network for taxi demand prediction. In: *Proceedings of the AAAI conference on artificial intelligence*
- Yuan H, Li G (2021) A survey of traffic prediction: from spatio-temporal data to intelligent transportation. *Data Science and Engineering* 6(1):63–85
- Zenkner G, Navarro-Martinez S (2023) A flexible and lightweight deep learning weather forecasting model. *Applied Intelligence* 53(21):24991–25002
- Zhang X, Jin Q, Yu T, et al (2022) Multi-modal spatio-temporal meteorological forecasting with deep neural network. *ISPRS Journal of Photogrammetry and Remote Sensing* 188:380–393



Zhou H, Hirasawa K (2019) Spatiotemporal traffic network analysis: technology and applications. *Knowledge and information systems* 60(1):25–61